

Crack-bridging behaviour of AR-glass multifilament yarns embedded in cement-based matrix – Modelling of ageing effects

M. Butler & V. Mechtcherine

Institute of Construction Materials, TU Dresden, Dresden, Germany

ABSTRACT: In this research project age-dependent changes in the crack-bridging behaviour of AR-glass multifilament yarns embedded in cementitious matrix were investigated at the meso and micro levels. Two cementitious matrices were considered where the binder contained Portland cement clinker. Mechanical characteristics of the bond between matrix and multifilament yarns after accelerated ageing were measured by means of double-sided yarn pullout tests. In these tests the multifilament yarns bridged a single crack in the matrix arising in a notched area of the specimen. Losses in crack-bridging performance with increasing age of composite were observed. The essential cause of such losses was discovered to be the microscopic densification of the fibre-to-matrix interface. This led to increased bond intensity and restricted slip-ability of the filaments. A phenomenological bond model was developed to relate these structural phenomena at the microscopic level to the mesoscopic material behavior. This cross-linkage model describes the crack-bridging effect of the entire multifilament yarn at the single filament level. According to the model, each filament possesses a specific deformation length depending on its position in the cross-section of the yarn. This deformation length depends on bond characteristics between single filament and cementitious matrix, which vary with age. Characteristic values of the model were computed from load-crack width curves obtained from the yarn pullout tests. The changes in the microstructure were represented by the characteristic values of the model.

1 INTRODUCTION

Textile-reinforced concrete (TRC) is a composite construction material consisting of high performance, multifilament yarns of glass or carbon fibre and a matrix of fine-grained concrete. In existing applications of TRC, chiefly fabrics made of alkali resistant glass fibres (so-called AR glass) are used. The main features of TRC are its high tensile strength and its pronounced ductile behaviour. TRC can be applied both in the fabrication of new structures and in the strengthening and repair of structural elements made of reinforced concrete or other traditional materials as well (Brameshuber 2006).

Most of these applications require that the high tensile strength and toughness of TRC do not degrade significantly with increasing age. Changes in the mechanical performance of the composite can result from deterioration of the armouring AR-glass fibres themselves due to the attack of OH⁻ ions in the pore solution (e.g. Paul 1977, Yilmaz et al. 1991, Hempel et al. 2007), the static fatigue (delayed failure) of the glass fibre under sustained load in the highly alkaline environment (e.g. Tomozowa 1996, Michalske et al. 1983, Purnell et al. 2001, Orłowski et al. 2008), and changes in the bond between matrix and fibres (e.g. Bartos et al. 1996, Zhu et al. 1997, Bentur 2000, Glinicki et al. 2007). The last-mentioned

effect results mainly from the densification of the matrix adjacent to the filaments and the intensified fibre-matrix bond with continued hydration. Furthermore, accumulation of hydration products at the interface between filaments and matrix and in the empty spaces between the filaments of multifilament yarn (bundle filling) can precipitate these alterations.

In this project the contribution of individual damage mechanisms to degradation of crack-bridging behaviour of multifilament yarn and their interaction is shown by means of a simple phenomenological model. The model is based on experimental data achieved from multifilament yarn pullout testing and micro-structural investigation of the yarn-matrix interface. A more extended and detailed presentation of the research work can be found in Butler (2009).

2 EXPERIMENTS

2.1 Test method – double-sided yarn pullout

The crack-bridging performance of multifilament yarn was evaluated using double-side pullout testing. In these pullout tests various artefacts resulting from a complex geometry of technical textiles is excluded, thus allowing a straightforward interpretation of the results obtained. Doubly symmetrical,

bone shaped prisms featuring a notch of depth 1mm in the middle were used as specimens. Each specimen was reinforced with three parallel oriented multifilament yarns extending over the entire length of the specimen. The amount of reinforcement was chosen in such way that multiple cracking was avoided and only single-crack formation at the notch occurred. The details on the test set-up and the specimens geometry may be found in Butler et al. (2009).

After demoulding one day after fabrication all specimens were stored for 6 days in water (20°C). Subsequently, one small part of specimens was subjected to reference storage (20°C/65% RH) until testing at an age of 28 days. The remainder of the test specimens was subjected to accelerated ageing in a fog room (40°C/99% RH). The periods of fog room storage were 28, 56, 90, 180 and 360 days.

The pullout testing was performed under controlled deformation conditions defined by a crack opening rate of 1mm/min.

2.2 Materials – yarn and fine-grained concrete

Multifilament yarn made of AR-glass (type CEM-FIL) was used as reinforcing material in the pullout tests. The multifilament yarn consists of 1600 individual filaments with a mean diameter of 13.6µm. The mean tensile strength of such filaments is 1917MPa and their mean strain capacity 0.0258.

A fine-grained concrete mixture M1 (cf. Table 1) is used as matrix material. The maximum aggregate diameter is 1mm. Compared to ordinary concrete the mixture has a high binder content.

Table 1. Composition of fine-grained concrete [kg/m³].

Matrix constituent	M1
CEM I 32,5 R	557
Fly ash	251
Microsilica*	56
Sand 0/1 mm	1114
Water	251

* Suspension; 50 M.-% powder, 50 M.-% water.

In the chosen matrix the appearance of Ca(OH)₂ (abbrev.: CH) and alkalis is controlled due to the presence of fly ash and microsilica in the binder. The pH decreases from an initial value of 12.6 to approximately 12.4 after 360 days of ageing.

2.3 Results of double-sided pullout tests

Here the characteristic pullout curves of specimens are shown. Each curve depicted represents a best-fit curve based on at least 7 individual pullout curves.

The pullout curves are represented in simplified fashion. The curve branches describing the un-cracked state of specimens are neglected and replaced by an interpolated line from $F(w=0) = 0$ to

the point where the yarn pullout is initiated, just after cracking of matrix. Likewise, the representation of the x-axis is simplified. It is not divided into axis intercepts for strain as well as for crack opening. Therefore the crack opening $w = 0$ is shifted to the left at the point where $F = 0$.

Figure 1 displays the characteristic pullout curves. The mechanical performance of the bond decreases with increasing duration of accelerated ageing. The maximum fibre pullout force decreases by approx. 40% after 360 days of accelerated ageing, whilst the pullout work during crack opening decreases by approx. 60% compared to the reference specimen. The tendency to decrease the maximum pullout force as well as pullout energy is more distinct in early ageing states than at higher composite age.

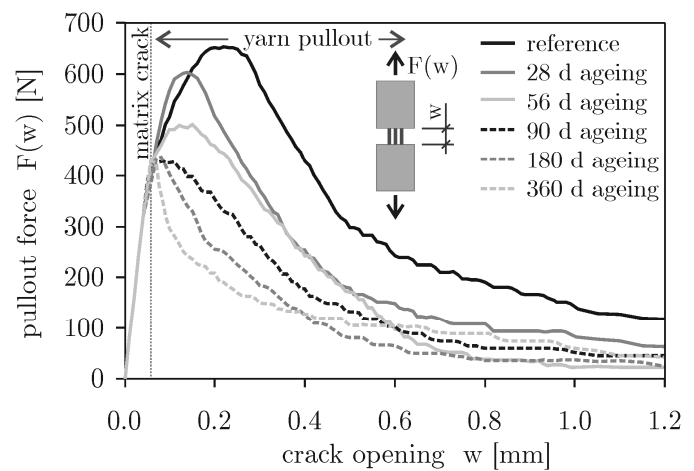


Figure 1. Force vs crack opening curves; storage at 40°C / 99% RH, reference at 20°C / 65% RH.

2.4 Results of micro-structural investigations

Figure 2 represents the characteristic microstructure in the interface between the multifilament yarn's sleeve filaments and matrix after 28 days' reference storage. The single filaments are embedded in an inhomogeneous matrix consisting of un-hydrated binder particles and hydration products. The matrix shows a structure which is not yet very dense. Contact between the hydration products and the filament surface is visible only at discrete points.

In Figure 3 the morphology of the same fibre-matrix-combination after 360 days' accelerated ageing is illustrated. Due to the ongoing hydration process the matrix becomes denser in comparison to Figure 2. The single filaments are covered by mineral incrustations mainly consisting of CSH phases. The hydration products on filament surface are much denser compared to Figure 2 and enclose the filament surface nearly on the entire surface. To a low extent also the formation of small CH crystals was substantiated by electron microscopy with associated EDX-analysis.

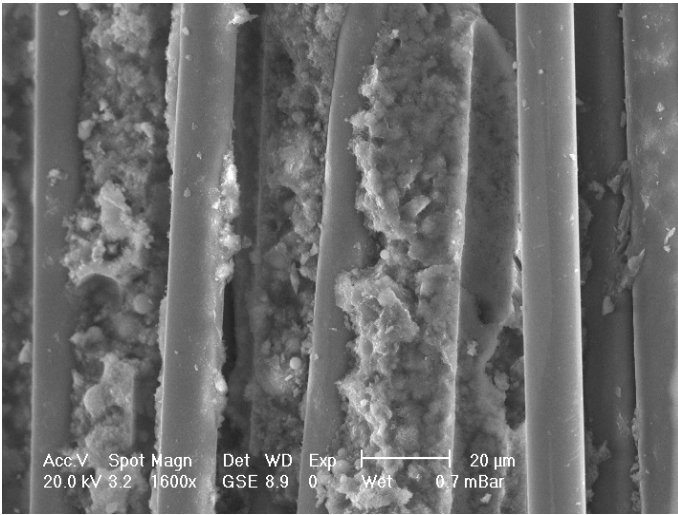


Figure 2. ESEM image of AR glass filaments in matrix M1, 28 days of reference storage (20°C / 65% RH).

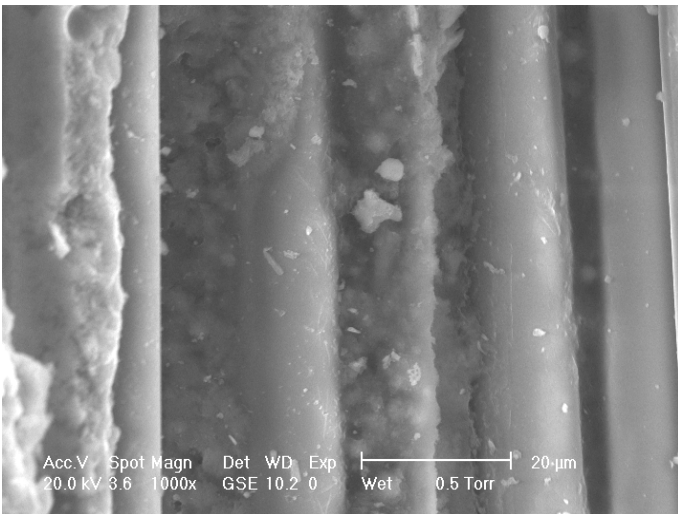


Figure 3. ESEM image of AR glass filaments in matrix M1, 360 days of accelerated ageing (40°C / 99% RH).

3 ADHESIVE CROSS-LINKAGE MODEL

3.1 Phenomenological basics of model

As shown in Section 2.4, the bond between filament and cementitious matrix is non-uniform. The hydration products form adhesive cross-links between matrix and filament or filament and filament, respectively (cf. Fig. 2). The bond properties of the cross-links depend on the characteristics of hydration products, which are influenced by the binder composition, the filament-sizing, and the condition and duration of hydration (e.g. Butler et al. 2009). However, the cross-links reduce or prevent the displacement of the filaments (e.g. Glinicki et al. 2007).

The basic idea of the adhesive cross-linkage model was proposed by Schorn (2003) and is based on the assumption that between two cross-links the filament can be deformed along the so-called available deformation length L_0 . In Figure 4 different types of bonding between filament and matrix and therefore different available deformation lengths are shown.

Due to the shear stiffness of adhesive cross-links and the linkage between filaments, an effective deformation length L_w is reduced, exceeding the available deformation length L_0 of the filament (cf. Fig. 4d). In the following the term “deformation length” is used synonymously with “effective deformation length”.

3.2 Distribution of deformation lengths

Because of the tiny distances between the filaments, the relatively large binder particles can not penetrate into the inner part of the multifilament yarn. Only hydration products can reach the yarn’s core. For this reason the frequency of cross-links decrease significantly from the sleeve filaments to the inner filaments.

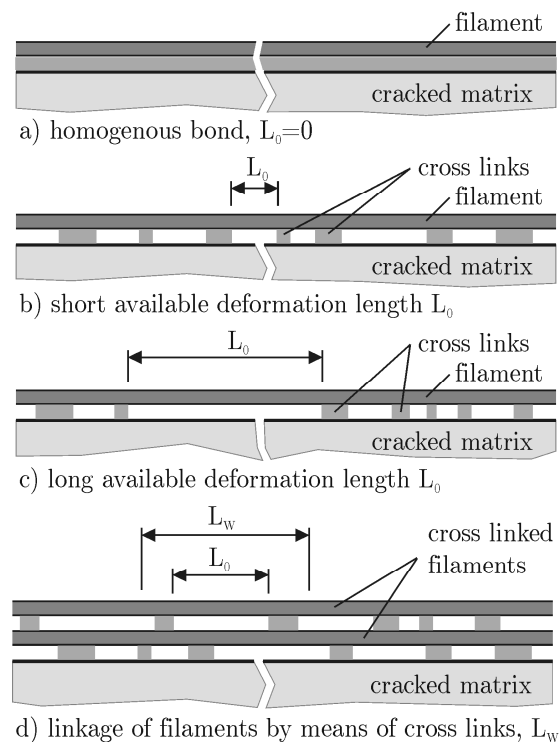


Figure 4. Different types of bonding represented by different available deformation lengths of filaments.

According to the cross-link model each filament has a specific deformation length depending on its position in the cross section of the yarn. In Figure 8 (left) a possible arrangement of deformation lengths over yarn diameter is sketched.

To model the crack-bridging behaviour of multifilament yarn, the indication of the deformation lengths of all filaments in the yarn becomes necessary. Figure 5 (right) illustrates a possible distribution of deformation lengths L_w . In this view the individual filament n is sorted according to its deformation length independent of its position in the yarn. The short deformation lengths of sleeve filaments are concentrated on top of the y-axis, the large deformation lengths of core filaments on the bottom.

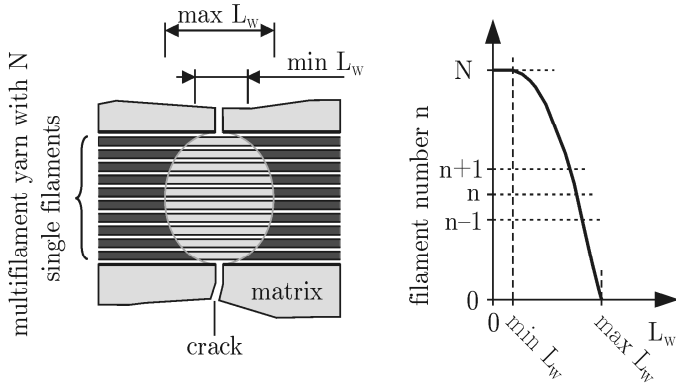


Figure 5. Arrangement of deformation lengths over diameter of yarn (left) and their distribution over filament number (right).

3.3 Modelling the yarn's crack-bridging behaviour

The deformation length of the filament determines the crack width at which the ultimate filament strain is reached. The filament stress at defined crack openings can be calculated according to Equation 1:

$$\sigma_n = E_n \varepsilon_n = E_n \frac{w}{L_{Wn}} \quad (1)$$

where σ = stress; E = young's modulus; L_W = deformation length of the filament, and w = crack width.

With increasing crack width w , the filaments fail little by little when each individual filament's strength is exceeded according to its deformation length. According to Equation 1, the stress level σ in a filament increases with decreasing L_W -value for a given crack-opening. Furthermore, cross-links can fail if their shear strength is exceeded before the maximum filament stress is reached. In this case, the associated deformation length increases. The crack-bridging load transferred by the entire multifilament yarn across the crack at crack width w can be determined according to Equation 2:

$$F = \sum_{n=1}^{N-n_f} F_n = \sum_{n=1}^{N-n_f} \sigma_n A_n = \sum_{n=1}^{N-n_f} A_n E_n \frac{w}{L_{Wn}} \quad (2)$$

where F = crack-bridging force; A = cross section of filament; N = total number of filaments; and n_f = number of failed filaments.

In Figure 6 the distribution of deformation lengths is indicated for a parabolic arrangement of deformation lengths around yarn diameter in a yarn with circular cross-section. At the yarn's core 10% of filaments are assumed inactive in crack-bridging load transfer; also cross-link failure is excluded. The resulting filament stresses, the crack-bridging load, and the number of failed filaments are indicated for crack width for both $w = 0.1w_{max}$ and $w = 0.5w_{max}$, respectively.

3.4 Recursive determination of distribution of deformation lengths

The adhesive cross-linkage model enables a specific correlation between the bonding situation of a multifilament yarn embedded in cementitious matrix and its mechanical behaviour when bridging a single crack. For computation of a load-crack width curve, knowledge of the distribution of the filaments' deformation lengths is indispensable. But the experimental determination of position, strength, and stiffness of cross-links between matrix and filament as well as between filaments is nearly impossible. The cross-links haven't an exact physical counterpart; they are rather an idealised abstraction of several bonding phenomena (cf. Section 3.1).

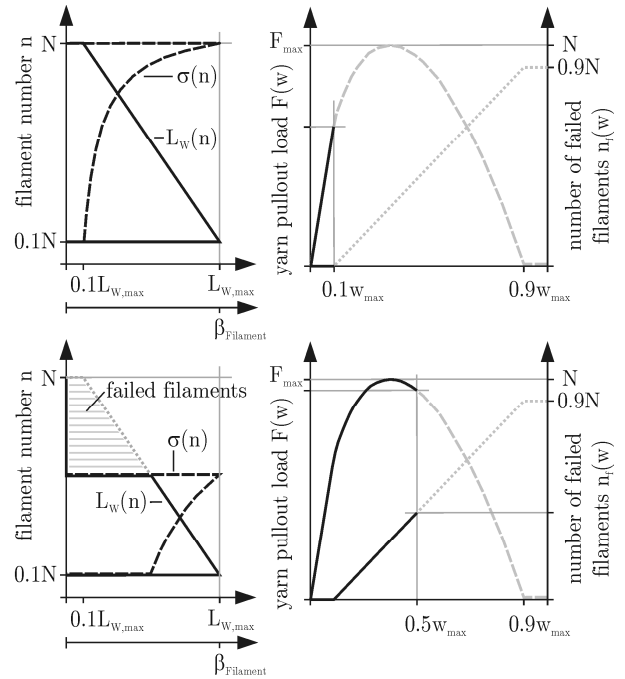


Figure 6. Deformation lengths of filaments L_w , filament stress σ , yarn pullout load F and number of failed filaments n_f for crack width $w = 0.1w_{max}$ (top) and $w = 0.5w_{max}$ (bottom).

However, the distribution of deformation lengths can be computed based on experimental data observed in pullout tests (cf. Section 2.1). In the initial phase of the recursive calculation process, it is assumed that all filaments have failed at crack width $w_{max} = w_U$, including the filaments possessing the maximum deformation length $L_{W,max}$. Hence, the number of intact filaments $M_U = 0$. At this point no further load is transmitted over the crack: $F_U = 0$. This initial state is summarised in Equation 3:

$$w = w_{max} = w_U ; F_U = M_U = 0 ; L_W = L_{W,max} = L_{W,U} \quad (3)$$

Before the state according to Equation 3 is reached, at crack with w_{U-1} a load F_{U-1} is transferred through M_{U-1} filaments. The deformation length of these filaments is $L_{W,U-1}$, where $L_{W,U-1} < L_{W,U}$. If Young's Modulus E and the cross section A of load bearing

filaments are known, their total number can be calculated according Equations 4 and 5:

$$w = w_{U-1} : F_{U-1} = E_F A_F \frac{w_{U-1}}{L_{W,V-1}} m_{U-1} \quad (4)$$

$$\rightarrow m_{U-1} = M_{U-1} = \frac{F_{U-1}}{E_F A_F w_{U-1}} L_{W,V-1} \quad (5)$$

Reducing the crack width by a further decrement at w_{U-2} , the crack-bridging load is F_{U-2} . The total number of intact filaments M_{U-2} is composed of the number of filaments m_{U-1} (which stay uncracked until crack width w_{U-1}) and the number of filaments m_{U-2} which fail during crack opening from w_{U-2} to w_{U-1} (cf. Fig. 9). At this point F_{U-2} results from the particular straining of both filament groups, m_{U-1} and m_{U-2} , respectively; see Equation 6. Considering the results of Equation 5, m_{U-2} can now be calculated according Equation 7:

$$w = w_{U-2} : F_{U-2} = E_F A_F \left(\frac{w_{U-2}}{L_{W,V-1}} m_{U-1} + \frac{w_{U-2}}{L_{W,V-2}} m_{U-2} \right) \quad (6)$$

$$\rightarrow m_{U-2} = \left(\frac{F_{U-2}}{E_F A_F w_{U-2}} - \frac{m_{U-1}}{L_{W,V-1}} \right) L_{W,V-2} \quad (7)$$

$$M_{U-2} = m_{U-1} + m_{U-2} \quad (8)$$

At any crack width w_{U-i} , where ($U > i > 1$), the crack-bridging load F_{U-i} is composed of i individual load components, resulting from m strained filaments inside each filament group (Equation 9, Fig. 7). The number of filaments m_{U-i} failing during crack opening from w_{U-i} to w_{U-i+1} can be calculated according to Equation 10 and the total number of intact filaments M_{U-i} using the corresponding Equation 11:

$$w = w_{U-i} : F_{U-i} = E_F A_F \left(\frac{w_{U-i}}{L_{W,V-1}} m_{U-1} + \frac{w_{U-i}}{L_{W,V-2}} m_{U-2} + \dots \right. \\ \left. \dots + \frac{w_{U-i}}{L_{W,V-i+1}} m_{U-i+1} + \frac{w_{U-i}}{L_{W,V-i}} m_{U-i} \right) \quad (9)$$

$$\rightarrow m_{U-i} = \left(\frac{F_{U-i}}{E_F A_F w_{U-i}} - \left[\frac{m_{U-1}}{L_{W,V-1}} + \frac{m_{U-2}}{L_{W,V-2}} + \dots \right. \right. \\ \left. \left. \dots + \frac{m_{U-i+1}}{L_{W,V-i+1}} \right] \right) L_{W,V-i} \\ = \left(\frac{F_{U-i}}{E_F A_F w_{U-i}} - \sum_{k=1}^{i-1} \frac{m_{U-k}}{L_{W,V-k}} \right) L_{W,V-i} \quad (10)$$

$$M_{U-i} = m_{U-1} + m_{U-2} + \dots + m_{U-i+1} + m_{U-i} = \sum_{k=1}^i m_{U-k} \quad (11)$$

To calculate the number of filaments m_{U-i} the specification of the deformation length of filaments $L_{W,V-i}$ is indispensable. This definition is based on the failure strain of filaments as shown in Equation 12:

$$\varepsilon_{F,f} = \frac{w_{U-i}}{L_{W,V-i}} \rightarrow L_{W,V-i} = \frac{w_{U-i}}{\varepsilon_{F,f}} \quad (12)$$

where $\varepsilon_{F,f}$ = failure strain of filaments.

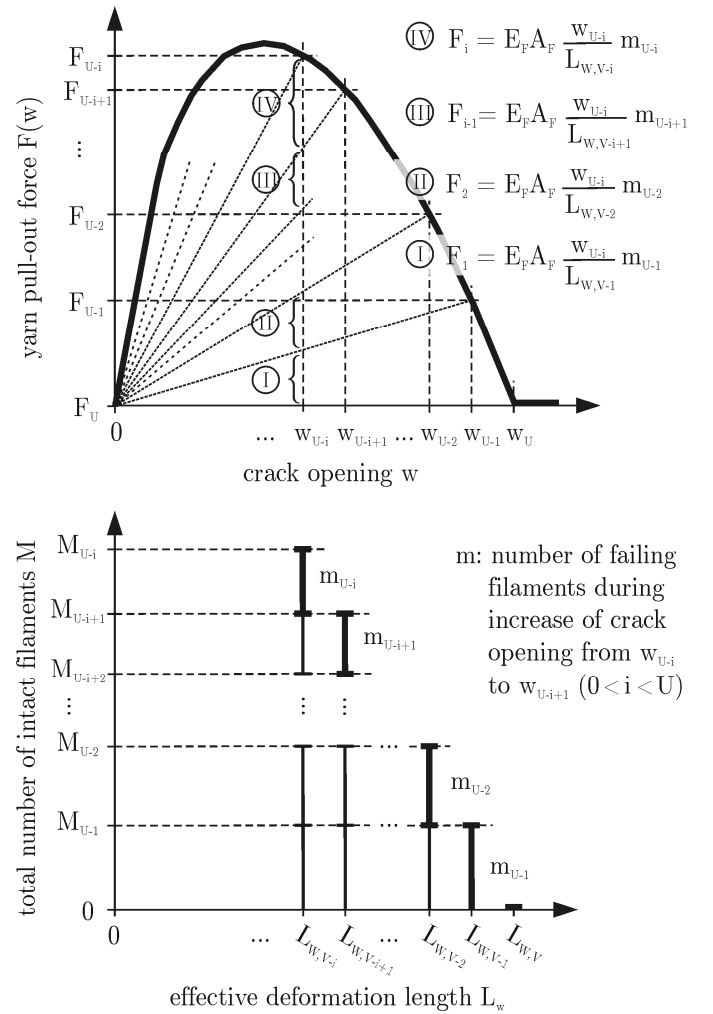


Figure 7. Sketch of calculation process of recursive determination of distribution of filament's deformation lengths based on measured pullout load-crack width curve.

The set of pair of values ($L_{W,V-i}$; M_{U-i}) resulting from the recursive computation according to Equation 10 represents the distribution of the filaments' deformation lengths inside the multifilament yarn bridging a single crack. To enable a graphic representation analogous to Figure 5 (right) the distribution-curve based on discrete pair of values ($L_{W,V-i}$; M_{U-i}) is transformed via linear interpolation to a quasi-continuous distribution curve based on pairs of values ($L_{W,V-i}$; n_j), where n = individual filament

number. The processing of this interpolation is depicted in Figure 8.

A calculated total number of filaments N_{calc} results from the numerical processing as described above. In the specimen the number of inactive filaments N_p can be determined by counting the filaments, which are pulled-out completely. Comparing $N_{calc} + N_p$ and the physical number of filaments in the yarn N , three cases must be distinguished:

a) $N_{calc} + N_p < N$: An iterative recalculation of $L_W(n)$ is performed with the stepwise reduced failure strain of filaments $\varepsilon_{F,f}$ until the condition $N_{calc} + N_p = N$ is satisfied. This case indicates a loss of filament strength, according to the reduction of $\varepsilon_{F,f}$.

b) $N_{calc} + N_p = N$: The calculation can be completed.

c) $N_{calc} + N_p > N$: The condition $N_{calc} + N_p = N$ can not be satisfied. This case indicates a cross-link breakdown instead of filament failure. The number of excessive filaments $N - (N_{calc} + N_p)$ and their deformation lengths indicate to what extent the breakdown of cross-links occurs (Butler 2009).

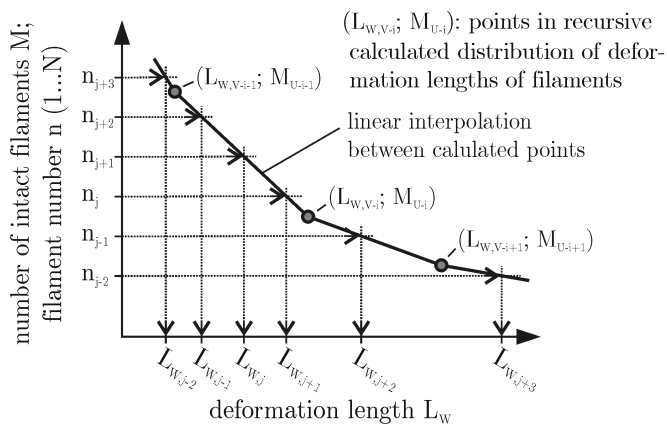


Figure 8. Determination of a quasi-continuous distribution-curve by means of linear interpolation between discrete points $(L_{W,V,i}; M_{U,i})$ resulting from recursive calculation process according to Figure 7.

4 APPLICATION OF CALCULATION MODEL ON EXPERIMENTAL RESULTS

The method of recursive calculation of distribution of deformation lengths (cf. Section 3.4) was used to conclude from experimental results (cf. Section 2.3) as to the bonding situation inside the multifilament yarn. A distribution curve of deformation lengths $L_W(n)$ was computed for each simplified pullout-crack width curve as pictured in Figure 1. In addition to the $L_W(n)$ -curves, filament strengths β_F are indicated, which were used to calculate the curves displayed.

In Figure 9 the results of the numerical processing of pullout data of matrix M1 specimens are shown. During ageing a decrease in the deformation lengths of almost all filaments can be reported. The minimal

deformation length $L_{W,min}$ at filament number $n = 4800$ is reduced from 7.5mm (reference curve) to 2mm (56d ageing). These reductions happen mainly in the sleeve filaments. Only the deformation lengths of core filaments ($n = 1 \dots$ approx. 300) show nearly no change with increasing age. From this state of ageing until an age of 360 days, the filament strength used in calculation was reduced from 1917MPa to 1451MPa to satisfy the condition $N_{calc} + N_p = N = 4800$. Only in reference specimens and after 28 days accelerated ageing higher numbers of filaments $N_{calc} + N_p$ were determined than were physically present in the yarn ($N = 4800$).

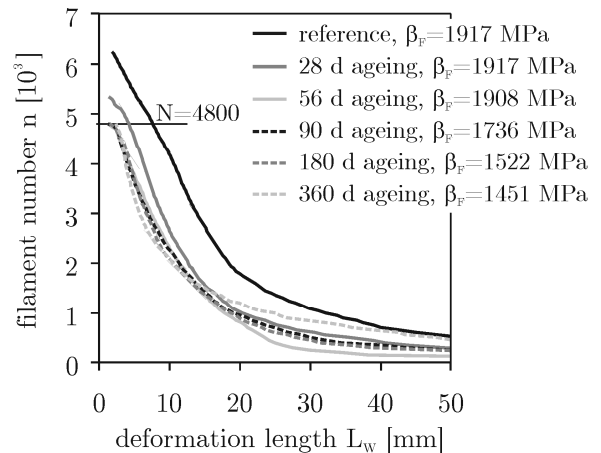


Figure 9. Calculated distribution of filament deformation lengths for matrix M1 specimens (based on Figure 1).

5 DISCUSSION OF RESULTS

At this point the results of mechanical testing (cf. Section 3.4), of numerical modelling (cf. Chapter 4), and of micro-structural investigation (cf. Section 2.4) can be discussed with a view to identifying the mechanisms which lead to the degradation in crack-bridging behaviour of multifilament yarn during ageing.

The reference specimens made of matrices M1 show favourable pullout behaviour. The well developed bond between filaments and matrices enables the slip of filaments relative to the matrix at high filament stress levels instead of filament failure and with that a high pullout work. This is substantiated by the distribution of deformation lengths, which indicate a significant potential for cross-link breakdown of reference specimen (cf. Fig. 9).

The tested specimens show a pronounced degradation of mechanical performance with age. During hydration process tiny slender CSH phases as well as relatively large and splittable CH phases are produced. A part of CH is transformed during pozzolanic reaction to CSH phases featuring a different morphology than CSH resulting from clinker hydration. Around the filament surfaces these hydration

products initially form thin-walled, slender wrappings, which become increasingly compact and stiffer, producing inflexible crusts. The rapid densification process in the matrix-filament interface with increasing age is substantiated by rapidly decreasing deformation lengths (Fig. 9). Thus, failure strain of the filaments is reached at smaller crack widths. Also the crusts restrict the slip of filaments in the vicinity of a matrix crack (no potential for cross-link breakdown from 56 day ageing, Fig. 9).

Furthermore, these brittle crusts can flake off locally if the covered filament is strained. At the points where the cross-section changes from a “composite-type”, consisting of filament and enveloping crust, to the original filament, high stress concentrations can arise due to the notch effect, which leads to the premature failure of the filament. This effect is represented by reduced strength of filaments β_F (cf. Fig. 9). Also, local notching of filament surface due to the less than critical growth of surface flaws (Purnell 2001, Orłowsky 2008) can not be excluded. These multiple effects explain the decrease in performance of aged specimens.

6 CONCLUSIONS

Degradations in mechanical performance of crack-bridging multifilament yarns can in the main be traced back to changes in the microstructure in the interface between matrix and filaments and between the filaments themselves, respectively. In addition to micro-structural investigations of interface morphology, this could be evidenced by means of modelling the time-dependent changes in distribution of filament deformation lengths $L_W(n)$. This distribution $L_W(n)$ can be computed from experimental pullout data according to a simple phenomenological model. With applicable identification of $L_W(n)$, densifications in the filament-matrix interface can be concluded, which reduce the deformability of filaments, hence causing a precipitate filament failure.

Furthermore, the changes in the morphology can lead to the decrease in filament strength. The causes of losses in filament strength can be both mechanical notching due to the scaling of mineral incrustations from the filament surface as well as the chemical notching of the filaments' bulk glass, referred to as the less than critical growth of surface flaws. Beside this the potential for cross-link breakdown can be estimated. It is an important composite feature to assure ductile crack-bridging through multifilament yarns at high load level.

ACKNOWLEDGEMENTS

The results were obtained in a project initiated in the Collaborative Research Centre SFB 528 “Textile Reinforcement for Structural Strengthening and Retrofitting” financed by the German Research Foundation “DFG”. The authors would like to acknowledge with gratitude the foundation's financial support.

REFERENCES

- Bartos, P.J.M. & Zhu, W. 1996. Effect of microsilica and acrylic polymer treatment on the ageing of GRC. *Cement Concrete Compos* 18(1): 31–9.
- Bentur, A. 2000. Role of interfaces in controlling durability of fiber-reinforced cements. *J Mater Civil Eng* 12(1): 2–7
- Bramshuber, W. (ed.) 2006. *Textile Reinforced Concrete. State-of-the-Art Report RILEM Technical Committee 201-TRC. RILEM Report 36, RILEM Publications S.A.R.L.*
- Butler, M. 2009. *Zur Dauerhaftigkeit von Verbundwerkstoffen aus zementgebundenen Matrices und alkaliresistenten Glasfaser-Multifilamentgarnen. Dissertation at the Institute of Construction Materials, TU Dresden, in German.*
- Butler, M., Mechtcherine, V. & Hempel, S. 2009. Experimental investigations on the durability of fibre–matrix interfaces in textile-reinforced concrete. *Cement & Concrete Composites* 31: 221-231.
- Glinicki, M.A. & Brandt, A.M. 2007. Quantification of glass fibre–cement interfacial properties by SEM-based push-out test. *Proc 5th int RILEM workshop high performance fiber reinforced cement composites, Proc 53 RILEM, 343–355.*
- Hempel, S. & Butler, M. 2007. Microscopic investigations on durability of textile reinforced concrete. *Proc 11th Euroseminar on microscopy applied to building materials, Porto.*
- Michalske, T.A. & Freiman, S.W. 1983. A molecular mechanism for stress corrosion in vitreous silica. *J Am Ceram Soc* 66(4): 284–8.
- Orłowsky, J. & Raupach, M. 2008. Durability model for AR-glass fibres in textile reinforced concrete. *Materials and Structures* 41(7): 1225-1233.
- Paul, A. 1977. Chemical durability of glasses; a thermodynamic approach. *J Mater Sci* 12(11): 2246–68.
- Purnell, P., Short, N.R. & Page, C.L. 2001. A static fatigue model for the durability of glass fibre reinforced cement. *J Mater Sci* 36(22): 5385–90.
- Schorn, H. 2003. Ein Verbundmodell für Glasfaserbewehrungen im Beton. *Bautechnik* 80(3): 174-180.
- Tomozawa, M. 1996. Fracture of glasses. *Annu Rev Mater Sci* 26: 43–74.
- Yilmaz, V. & Glasser, F. 1991. Reaction of alkali-resistant glass fibres with cement. Part 2: durability in cement matrices conditioned with silica fume. *Glass Technology* 32(4): 138–47.
- Zhu, W. & Bartos, P.J.M. 1997. Assessment of interfacial microstructure and bond properties in aged GRC using a novel microindentation method. *Cem Concr Res* 27(11): 1701–11.